



Cite this: DOI: 10.1039/c5cy02248g

Role of alkali earth metals over Pd/Al₂O₃ for decarbonylation of 5-hydroxymethylfurfural†

Qingwei Meng,^{ab} Chengwu Qiu,^{ab} Guoqiang Ding,^c Jinglei Cui,^{ab} Yulei Zhu^{*ac} and Yongwang Li^{ac}

A series of Pd/Al₂O₃ catalysts with different alkali earth metals (Mg, Ca, Sr, Ba) and varying Sr loadings (1.8, 3.5, 5.3, 7 and 8.8 wt%) were investigated for 5-hydroxymethylfurfural (HMF) decarbonylation. The alkali earth metal and content were demonstrated to have profound influences on the metal dispersion, electron density of the metal, acid–base properties of the catalyst, and catalytic performance. The Pd3Sr/Al₂O₃ catalyst exhibited the highest initial activity and furfuryl alcohol selectivity, achieving a yield of 92%. The key to high decarbonylation selectivity is the suppression of hydrogenolysis and etherification side reactions through the attenuation of the acidity of catalysts. Successful catalytic activity not only lies in the increased metallic surface area, but is also affected by the adsorption properties of the carbonyl group and the poisoning CO produced. The catalytic activity is linearly correlated to the surface metallic area at low modifier loading over PdM/Al₂O₃ catalysts. But along with further increased metallic surface area over PdXSr/Al₂O₃, HMF conversion initially increased, reaching a plateau over Pd3Sr/Al₂O₃ and then decreased with increasing Sr loading. A synergistic effect between the Sr species and metallic Pd was proposed, which promoted the migration of carbonyl adsorption from the support to the surface Pd through the electron donation of Sr species to Al₂O₃ and metallic Pd.

Received 23rd December 2015,
Accepted 1st February 2016

DOI: 10.1039/c5cy02248g

www.rsc.org/catalysis

1. Introduction

Fossil energy depletion and global warming have stimulated extensive attention to the conversion of biomass to fuels¹ and chemicals.² The technology of utilizing biomass is based on the development of a versatile and selective catalytic defunctionalisation processes.^{1b,c,2d,3} In general, the highly oxygenated carbohydrates put severe constraint on the conversion of biomass to fuels. In order to reduce the oxygen content, hydrogenation and hydrogenolysis, usually sequentially, are often performed.⁴ However, selective decarbonylation and decarboxylation are far less developed at present.

Furfuryl alcohol (FOL) is widely used in the fine chemical and polymer industries. The main applications of FOL are the production of resins, synthetic fibers, farm chemicals, fine chemical products such as Vitamin C and tetrahydrofurfuryl alcohol, *etc.*⁵ Presently, FOL is produced by hydrogenation of furfural (FAL). Furfural is already produced on an industrial scale from hemicelluloses (polymers of C₅

sugars) depending on the well developed conversion technology.^{2d,3a,6} Given the greater availability and versatility of C₆ over C₅ sugars in biomass feedstock, it seems critical to establish an integrated process network to utilize C₆ sugars. HMF, which is an important platform chemical for the conversion of C₆ sugars, is converted from cellulose.^{2d,7} The prospective availability of large scale and cheap HMF necessitates further development in its process chemistry. Conversion technology for oxidation,⁸ hydrogenation⁹ and etherification¹⁰ of HMF has been reported. HMF decarbonylation to FOL can be envisaged as another way to utilize the C₆ sugars.

HMF decarbonylation was first reported by Larry D. Lillwitz in alkali systems containing alkali metal or alkaline earth metal salts to modify the homogenous or heterogeneous catalysts at subatmospheric pressure,¹¹ which suffer from the need for a stoichiometric amount of active metal species or low selectivity. Recently, Leitner *et al.*¹² reported a highly selective decarbonylation by using a homogeneous compound [IrCl(cod)]₂PCy₃ at 220 °C in the presence of compressed CO₂ (50 bar). Later, Fu *et al.*¹³ carried out the same reaction using a heterogeneous Pd/SBA-15 catalyst at 140 °C necessarily in the presence of molecular sieves. Whereafter, Rauchfuss *et al.* decreased the decarbonylation temperature to 120 °C by using an open system over Pd/C.¹⁴ But the open system involving the highly active HMF and the reduced

^a State Key Laboratory of Coal Conversion, Institute of Coal Chemistry, Chinese Academy of Sciences, Taiyuan 030001, PR China. E-mail: zhuyulei@sxicc.ac.cn; Fax: +86 351 7560668; Tel: +86 351 7117097

^b University of Chinese Academy of Sciences, Beijing 100039, PR China

^c Synfuels China Co., Ltd., Beijing 101407, PR China

† Electronic supplementary information (ESI) available. See DOI: 10.1039/c5cy02248g

catalyst may be threatened by oxygen in air. A simple and universal catalytic system involving conventional catalysts is desired. Pd/Al₂O₃ is the most effective and widely used supported Pd catalyst for decarbonylation reactions though it has not been used for HMF decarbonylation.¹⁵ But as HMF and the decarbonylation product FOL are highly reactive and the functional groups are sensitive to acidic environment,¹¹ the acidic Al₂O₃ may restrict its application for HMF transformation. Based on this consideration, the decarbonylation performance in a closed system over Pd/Al₂O₃ is expected to be promoted by modulating the surface acidity.

The Ca in the PtSn/ZSM-5 catalyst weakened the acidity and suppressed coke deposition.¹⁶ Zhang *et al.* found that the acid sites of the Cu/SiO₂ catalyst were neutralized by the addition of alkali earth metals (Ca, Sr, Ba) and the dispersion of metal was also improved resulting in increased catalytic activity.¹⁷ Nieuwenhuys *et al.*¹⁸ found that alkali earth metals decreased the size of gold particles and prevented the small particles from sintering. Besides their influences on acid–base properties and metal dispersion, alkali earth metals also impact on the electronic structure. Musolino *et al.*¹⁹ have found that the promoters K, Ca, Ba affect the reducibility and the electronic properties of the Ru/SiO₂ sample. It is revealed by a report from our group that the doping of K to Pd/Al₂O₃ promoted the furfural decarbonylation because of the different adsorption mode and adsorption intensity of furfural on doped and undoped samples caused by electron intensity changes.¹⁵ Thus, not only the acid–base properties, but also the metal dispersion, electronic structure and the adsorption properties of catalysts may be modified by addition of alkali earth metals to Pd/Al₂O₃ and the decarbonylation performance is expected to be improved.

In this work, Pd/Al₂O₃, which has potential for industry but is not beneficial to the conversion of HMF, was firstly used for HMF decarbonylation. We focus on the effect of different alkali earth metals (Mg, Ca, Sr, Ba) as well as varying Sr loading on both surface characteristics of Al₂O₃ supported Pd catalyst and its catalytic performance. It can be shown that the doping of Sr species to Pd/Al₂O₃ exhibits the best catalytic performance among the different kinds of additives. Introducing an optimal Sr amount to Pd/Al₂O₃ can enhance surface Pd dispersion, increase metallic surface area, balance moderate adsorption strength of CO and carbonyl group on metallic Pd, attenuate the surface acidity of the catalyst to a rather low extent, and therefore, greatly improve the catalytic activity and FOL selectivity.

2. Experimental

2.1. Catalyst preparation

All the catalysts were prepared by the incipient wet impregnation method. Firstly, M/Al₂O₃ (M = Mg, Ca, Sr, Ba) and XSr/Al₂O₃ (X = 2, 3, 4, 5) supports were prepared by impregnating the parent Al₂O₃ powders (Aluminum Co., Ltd, of China) with an aqueous solution of alkali earth metal nitrate (Sinopharm Chemical Reagent Co., Ltd) for 5 h, followed by drying at 80

°C for 16 h and calcinating at 400 °C for 2 h. Then, the powders obtained were respectively impregnated with calculated Pd(NO₃)₂ aqueous solution. PdM/Al₂O₃ and PdXSr/Al₂O₃ catalysts were obtained by repeating the above drying and calcinating procedures. The molar amount of the alkali earth metals in PdM/Al₂O₃ catalysts were 0.2 mmol g⁻¹. X denotes the folds of Sr content in PdXSr/Al₂O₃ compared to that in PdSr/Al₂O₃. Other catalysts were prepared a single impregnation step. The nominal Pd loading of all the catalysts except x (x = 0.5, x = 2, x = 3) % Pd/Al₂O₃ is 1 wt%.

2.2. Catalyst characterization

The BET surface area (S_{BET}), pore size (D_{p}) and pore volume (V_{p}) were determined *via* N₂ physisorption at -196 °C using a Micromeritics ASAP 2420 instrument. The samples were degassed under vacuum at 90 °C for 1 h and 350 °C for 8 h prior to the measurement.

The concentration of the metal in the catalysts was determined by induced coupled plasma-optical emission spectrometry (ICP-OES, Thermo iCAP 6300, USA).

Pd dispersion and surface metal area were measured by CO chemisorption using dynamic pulse technique on Auto Chem. II 2920 equipment (Micromeritics, USA) at 50 °C using a pulse of 5% CO in He. Prior to the measurement, the samples were reduced *in situ* by flowing H₂ at 200 °C for 2 h and heated to 250 °C in He for 30 min to remove hydrogen species adsorbed on the surface. The Pd dispersion was calculated assuming an adsorption stoichiometry of one CO per exposed palladium atom.

Temperature programmed reduction (TPR) was conducted on a TP-5080 (Tianjin Xianquan Industry and Trade Development Co., LTD) with a TCD detector. In a typical experiment, 30 mg of the catalyst were placed in a quartz microreactor and were heated from 20 °C to 600 °C in 5% H₂/N₂ mixture after baseline stabilization.

The *in situ* CO-FTIR was performed on an infrared spectrometer (VEREX70, Bruker, Germany). Prior to the adsorption of CO, the catalysts were reduced in H₂ flow (20 ml min⁻¹) at 200 °C for 2 h, purged with He for 0.5 h and cooled down to 30 °C. Then the samples were purged with helium and the CO-FTIR spectra were recorded.

The *in situ* Furfural-FTIR was collected on the same infrared spectrometer with the CO-FTIR. Prior to the tests, the catalysts were reduced *in situ* at 200 °C for 2 h and then cooled to 30 °C. Furfural vapor was pulled through the chamber by a vacuum pump for the measurement and the spectra were recorded. After that, Furfural-FTIR spectra were again recorded after applying a vacuum and at different temperatures.

The acidity and basicity of the catalysts were measured with thermal programmed desorption (TPD) of NH₃ and CO₂ respectively on Auto Chem. II 2920 equipment (Micromeritics, USA) with a mass spectrometer. Prior to each measurement, 200 mg of sample was reduced *in situ* by flowing H₂ at 200 °C for 2 h, and then purged with He for 1 h. After

cooling to 100 °C under a continuous flow of helium, the sample was adsorbed with NH₃ or CO₂ until saturation. Then, the catalyst was subsequently flushed with helium at 100 °C for 0.5 h to remove the physisorbed NH₃ or CO₂. TPD was conducted from 100 °C to 800 °C at a heat rate of 10 °C min⁻¹.

2.3. Activity test and analysis method

Decarbonylation of HMF was performed in a 50 mL stainless steel autoclave at a stirring speed of 300 rpm. All the catalysts were used in the particle form with a granule size of 20 to 40 mesh. Prior to each test, the samples were reduced with an H₂ flow at 200 °C for 2 h. In a typical run, 1.2 g HMF (Shanghai DEMO Medical Tech. Co., Ltd, China), 25 g 1,4-dioxane, and 0.25 g catalysts were introduced into the autoclave. Afterwards, the reactor was purged with N₂ seven times to replace the air in the autoclave, and then heated to 180 °C. After the reaction, the autoclave was cooled down rapidly using an ice-water bath. The gas was collected and analyzed off-line by two gas chromatographs (GCs) (models 6890N, Agilent, USA) equipped with a flame ionization detector (FID) and a thermal conductivity detector (TCD) respectively. The liquid products were separated by removing the catalyst with filtration and analyzed by a GC (model 6890N, Agilent) equipped with a FID detector. The furan-derived products in the gaseous phase can be neglected with a content of less than 1% as determined by the gaseous analysis. The conversion and the selectivity were determined based on the area normalization method. The content of FOL, 2-methylfuran (2-MF), FAL, 5-methylfurfural (MFAL) and HMF were also tested by an external standard method which was normalized by the area of the solvent. The results calculated by the two methods were consistent.

3. Results

3.1. HMF decarbonylation over different supported Pd catalysts

Initially, several metal oxides including Al₂O₃, TiO₂, ZnO and SiO₂ were applied as the supports of Pd catalysts (Table 1 entries 1–4). Besides the decarbonylation product FOL, a lot of

side products were also detected due to the high activity of HMF itself, such as difurfuryl ether (DFE), 2-MF, 2,5-dimethylfuran (DMF) and MFAL, which has not been reported for HMF decarbonylation. As shown in Scheme 1, the main byproducts could be attributed to four pathways: (1) etherification of FOL forming DFE, (2) generation of 2-MF, DMF and MFAL through hydrogenolysis of C–O bond, (3) dehydrogenation of FOL or hydrogenolysis of the C–CH₂OH bond in HMF producing FAL, (4) opening or connecting of the furan ring. The H₂ involvement in the side reactions may be derived from (1) the water-gas shift (WGS) reaction (trace water could be derived from the solvent and the moisture in HMF), (2) H₂ adsorption on catalysts during reduction, or (3) dehydrogenation of the reaction system. Hydrogen from WGS and adsorption on catalysts were detected (data see Table S1[†]). Among the different supported Pd catalysts, the Pd/Al₂O₃ catalyst exhibits the best catalytic activity and FOL selectivity. Pd/ZnO shows almost no activity, while the initial activity of Pd/TiO₂ is also quite low compared with Pd/Al₂O₃. The FOL selectivity over Pd/SiO₂ is a lot lower than that over Pd/Al₂O₃ as a large amount of hydrogenolysis and etherification byproducts were formed. XRD and TEM were performed to investigate the relationship between the activity and dispersion. No diffraction peak due to Pd for the four reduced samples (Fig. S1[†]) implies that Pd is highly dispersed on the four supports.

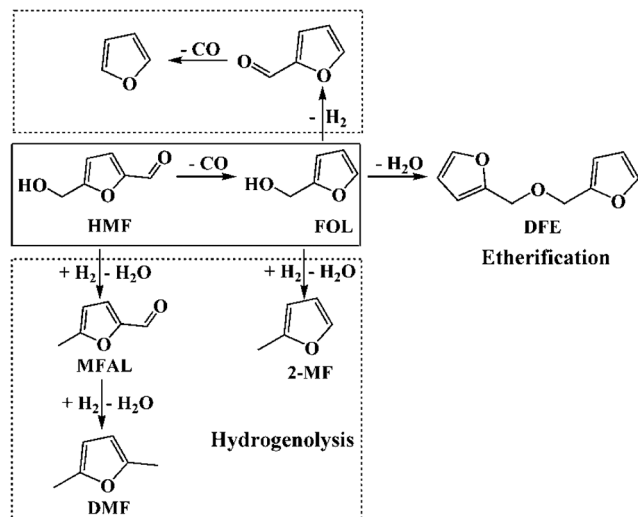
However, TEM results (Fig. S2[†]) after reduction show that Pd nanoparticles on Pd/SiO₂ (with an average crystal size of 5.5 nm) and Pd/TiO₂ (6.5 nm) are larger than that on Pd/Al₂O₃ (4.5 nm), resulting in the lower activity of Pd/SiO₂ and Pd/TiO₂. Small particles were found to be beneficial to decarbonylation.²⁰ The particle size of Pd on Pd/ZnO (4.5 nm) is the smallest but with uneven dispersion (Fig. S2[†]). The low activity of Pd/ZnO may result from the uneven dispersion and the weak acid–base properties. Conclusively, appropriate acid–base properties and smallest particle size resulted in the highest activity of Pd/Al₂O₃.

Moreover, the effect of metal loading was also investigated as shown in Table 1 entries 4–7. An increase of 0.5–1 wt% in the Pd loading causes the dramatic promotion of the catalytic activity. The further elevation of metallic loading only results

Table 1 Effects of supports and metallic loading on catalytic decarbonylation of HMF^a

Entry	Cat.	Conv. (%)	Selectivity ^b (%)				
			FOL	FAL	DFE	Hydrogenolysis 2-MF+DMF+MFAL	Others
1	Pd/SiO ₂	53.0	40.9	6.4	3.0	31.4	18.4
2	Pd/ZnO	2.9	19.9	6.8	4.5	25.7	25.3
3	Pd/TiO ₂	23.3	56.1	10.2	2.4	27.5	3.3
4	Pd/Al ₂ O ₃	61.8	65.7	11.2	9.1	8.2	5.8
5	0.5% Pd/Al ₂ O ₃	47.8	60.8	12.9	11.4	9.2	5.7
6	2% Pd/Al ₂ O ₃	63.5	76.1	7.1	3.4	10.8	2.6
7	3% Pd/Al ₂ O ₃	71.0	74.2	8.7	3.1	9.6	4.4

^a Conditions: 1.2 g HMF, 25 g 1,4-dioxane, 0.25 g catalyst, N₂ atmospheric pressure (room temperature), *T* = 180 °C, *t* = 16 h. ^b FOL = furfuryl alcohol, FAL = furfural, DFE = difurfuryl ether, 2-MF = 2-methylfuran, DMF = 2,5-dimethylfuran, MFAL = 5-methylfurfural, others mainly include furan, ring-opening products and oligomers.



Scheme 1 Reaction pathways for the conversion of HMF over Pd catalysts.

in slight increase of conversion. Different from the tendency of activity, the FOL selectivity increased gradually from 60% to 76% with increased Pd loading in the range 0.5–2 wt%. The FAL selectivity shows an adverse trend with that of FOL. The selectivity of FOL and FAL over 2 wt% Pd/Al₂O₃ is similar with that over 3 wt% Pd/Al₂O₃. Besides the target FOL, the main side products were produced through hydrogenolysis and/or etherification which can be facilitated by the acid centers over the surface.²¹ So suppression of the side reactions was conceived of by addition of alkali earth metals to Pd/Al₂O₃ through the modification of the surface acidity.

3.2. Doping effects of alkali earth metals on Pd/Al₂O₃ for HMF decarbonylation

A comparative test over Sr-modified Al₂O₃ (2 wt% Sr loading on Al₂O₃) was also carried out at 180 °C, showing no

observable conversion of HMF. The results of the alkali earth metal-added PdM/Al₂O₃ (M = Mg, Ca, Sr, Ba) and PdXSr/Al₂O₃ catalysts are displayed in Table 2. Not only the catalytic activity but also the product selectivity is influenced significantly by the doping of alkali earth metals. Depending on the different additives, the catalytic performance of the PdM/Al₂O₃ catalyst is improved to different extents. The HMF conversion increases in the order: Pd/Al₂O₃ < PdMg/Al₂O₃ < PdCa/Al₂O₃ < PdSr/Al₂O₃ < PdBa/Al₂O₃. However, the selectivity of the hydrogenolysis/etherification products and FAL selectivity shows an adverse trend with the activity, indicating that the side reactions are suppressed upon the increase of the basic strength of the pure alkali earth metal oxides. As a result, FOL selectivity gradually increases. Though the conversion of PdBa/Al₂O₃ is higher than that of PdSr/Al₂O₃, the FOL selectivity of PdBa/Al₂O₃ is lower because of more ring-opening products. Thus, the addition effect of Sr was further investigated.

To further improve the catalytic performance, the effect of the dopant loading was investigated. The catalytic activity and product selectivity of PdXSr/Al₂O₃ catalysts are displayed in Table 2. The addition of Sr significantly enhances the initial HMF conversion. There appears to be an optimal Sr loading, beyond which further increases in Sr loading lead to a decrease in the catalytic activity. Pd3Sr/Al₂O₃ shows the highest HMF conversion as well as the highest level of FOL selectivity. Different from the tendency of catalytic activity, the FOL selectivity over PdXSr/Al₂O₃ catalysts initially increases with the elevated Sr loading over Pd/Al₂O₃–Pd3Sr/Al₂O₃ (Table 2 entries 1, 4, 6, 7) and remains at the same level as that over Pd3Sr/Al₂O₃ with a further increase in Sr loading (Table 2 entries 7–9). On the contrary, the hydrogenolysis, etherification and FAL selectivity decreases upon increasing Sr loading until the selectivity of FOL reaches a maximum, indicating that the excess of Sr could not suppress etherification and hydrogenolysis further. As the produced CO is poisoning and hinders decarbonylation, gas exchange was conducted during the reaction to complete the

Table 2 HMF decarbonylation over different alkali earth metal-doped Pd/Al₂O₃^a

Entry	Cat.	Conv. (%)	Selectivity ^b (%)				
			FOL	FAL	DFE	Hydrogenolysis 2-MF+DMF+MFAL	Others
1	Pd/Al ₂ O ₃	61.8	65.7	11.2	9.1	8.2	5.8
2	PdMg/Al ₂ O ₃	66.6	72.0	10.4	4.6	6.4	6.6
3	PdCa/Al ₂ O ₃	71.9	75.5	8.9	2.8	5.3	7.5
4	PdSr/Al ₂ O ₃	76.9	80.7	8.3	1.9	4.9	4.2
5	PdBa/Al ₂ O ₃	79.0	77.8	7.4	2.1	4.2	8.5
6	Pd2Sr/Al ₂ O ₃	83.7	84.2	6.7	0.8	3.3	5
7	Pd3Sr/Al ₂ O ₃	91.1	91.1	3.7	1.2	1.9	2.1
8	Pd4Sr/Al ₂ O ₃	84.9	92.0	3.6	0.8	1.8	1.8
9	Pd5Sr/Al ₂ O ₃	82.3	91.8	4.3	0.7	1.8	1.4
10 ^c	Pd3Sr/Al ₂ O ₃	100	92.3	3.6	1.0	1.2	1.9
11 ^c	Pd/Al ₂ O ₃	70.2	70.5	10.1	8.7	7.8	2.9

^a Conditions: 1.2 g HMF, 25 g 1,4-dioxane, 0.25 g catalyst, N₂ atmospheric pressure (room temperature), *T* = 180 °C, *t* = 16 h. ^b FOL = furfuryl alcohol, FAL = furfural, DFE = difurfuryl ether, 2-MF = 2-methylfuran, DMF = 2,5-dimethylfuran, MFAL = 5-methylfurfural, others mainly include furan, ring-opening products and oligomers. ^c Reaction for 8 h, cooled down and purged with fresh N₂, reaction for another 8 h.

conversion of HMF. After purging with fresh N_2 once at the middle of the reaction, Pd3Sr/Al₂O₃ achieved a FOL yield of 92% (Table 2 entry 10). The CO poisoning effect on Pd/Al₂O₃ was also demonstrated by purging with fresh N_2 in the middle reaction as shown in Table 2 entry 11. Decarbonylation of FAL was also performed over PdXSr/Al₂O₃ catalysts, exhibiting a similar conversion tendency with that of HMF (see Table S2†).

Pd3Sr/Al₂O₃ was reused for several runs successively (Fig. 1) and maintained the initial activity and FOL selectivity, indicating good stability and reusability.

3.3 Characterization of catalysts

3.3.1 Physicochemical properties of catalysts. The physicochemical properties of the PdM/Al₂O₃ and PdXSr/Al₂O₃ catalysts are summarized in Table 3. The Al₂O₃ shows a high BET surface area, while a slight decrease is observed for the Pd/Al₂O₃ catalyst due to the deposition of metal Pd. The S_{BET} and the pore volume of the PdBa/Al₂O₃ catalyst is apparently

decreased in comparison with that of the Pd/Al₂O₃ catalyst, while no noticeable changes in the textural characteristics can be observed for other PdM/Al₂O₃ catalysts. This may be the reason that Ba contains the biggest atomic radius resulting in the most obvious covering and blocking effect. With an increase in Sr content in the range of 2–10%, the surface area and pore volume of the catalysts shows a gradual decrease. Pd5Sr/Al₂O₃, specifically, shows a significant decrease and has the lowest values of surface area and pore volume. The decrease is probably due to surface covering and pore blocking of support caused by addition of Sr additive, similar to previous reports of different additive content on the textural properties of the support.²² Pd loadings of all catalysts determined by ICP analysis is similar ($\approx 0.85\%$) and is slightly lower than the nominal value of 1%. The loading of the additives in PdM/Al₂O₃ is similar to the nominal value, while Sr content in PdXSr/Al₂O₃ is lower than the nominal loading of 2%, 4%, 6%, 8%, and 10%. XRD experiments were conducted (Fig. S3†), but all the reduced samples only exhibited a diffraction peak due to Al₂O₃, implying the fine dispersion of metal Pd or the poor crystallinity. CO chemisorption is an important method to characterize metal dispersion and metallic surface area, which are closely related to the catalytic performance of supported metal catalysts.²³ The Pd dispersion and metal area were calculated from the volume of the pulse chemisorption of CO. It has been demonstrated that the amount of CO consumed over the catalysts is adsorbed solely on the surface Pd component.^{23a} The Pd dispersion and metal area increases with the basic strength of the additives for PdM/Al₂O₃ catalysts and increases continuously with elevated Sr loading, reaching the maximum level over Pd4Sr/Al₂O₃ and Pd5Sr/Al₂O₃. Generally, sintering is the main reason for the agglomeration of metal component and results in a decrease in metal dispersion and surface area. Depending on different additives and adding content, the sintering resistance of the catalyst can be improved to some extent under reduction conditions.

3.3.2 H₂-TPR. TPR experiments are generally used to investigate the reducibility of the species present on the support. It is possible to determine whether the dopants have interacted with the supported Pd²⁺ precursor or not (before or

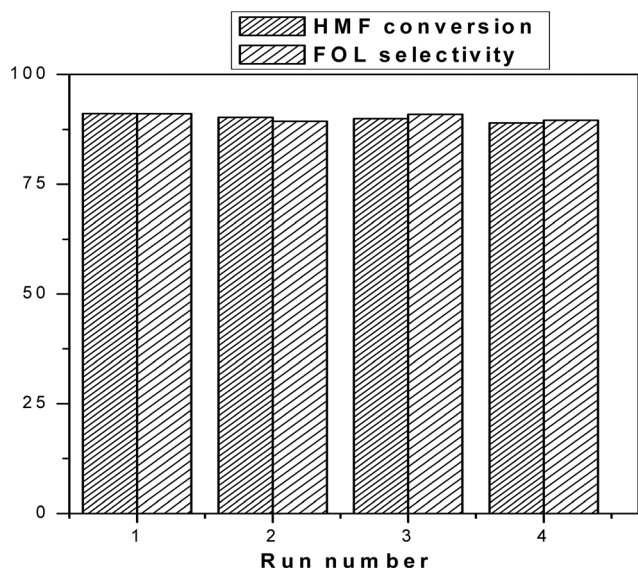


Fig. 1 The stability of the Pd3Sr/Al₂O₃ catalyst. Conditions: 1.2 g HMF, 25 g 1,4-dioxane, 0.25 g catalyst, N_2 atmospheric pressure (room temperature, RT), $T = 180^\circ C$, $t = 16$ h.

Table 3 Main physicochemical properties of the catalysts

Catalysts	Metal loading ^a		S_{BET}^b (m ² g ⁻¹)	V_p^b (cm ³ g ⁻¹)	D_p^b (nm)	Dispersion ^c (%)	Metallic surface area ^c (m ² g ⁻¹ metal)
	Pd (wt%)	Promoters (wt%)					
Al ₂ O ₃	—	—	199	0.7	10.8	—	—
Pd/Al ₂ O ₃	0.9	—	179	0.7	11.4	19	75
PdMg/Al ₂ O ₃	0.8	0.6	178	0.7	11.2	23	90
PdCa/Al ₂ O ₃	0.8	1.2	182	0.7	11.1	27	105
PdSr/Al ₂ O ₃	0.8	2.0	179	0.6	11.1	29	115
PdBa/Al ₂ O ₃	0.8	3.0	156	0.5	10.9	30	118
Pd2Sr/Al ₂ O ₃	0.8	3.8	163	0.6	11.0	34	132
Pd3Sr/Al ₂ O ₃	0.8	5.8	156	0.6	10.7	36	141
Pd4Sr/Al ₂ O ₃	0.8	7.2	151	0.6	10.7	38	150
Pd5Sr/Al ₂ O ₃	0.8	8.6	138	0.5	10.7	39	150

^a Determined by ICP-OES. ^b Determined by BET method. ^c Determined by CO-chemisorption.

during reduction) by comparing the TPR results of the undoped with doped samples.²⁴ The H₂-TPR profiles for different alkali earth metal-doped PdM/Al₂O₃ catalysts and for different Sr loadings of PdXSr/Al₂O₃ samples are shown in Fig. 2. All the samples (except Pd5Sr/Al₂O₃) show a single low temperature reduction peak, which is assigned to the Pd²⁺ → Pd⁰ reduction peak.¹⁵ But a peak at 192 °C appears over the Pd5Sr/Al₂O₃ catalyst, which could be ascribed to the reduction of nitrates due to a high loading of Sr nitrate (see Fig. S4 and S5† for detail). The hydrogen consumption, quantitatively measured from TPR, is approximately equivalent to the Pd loading amount (see Table S3†). The negative H₂ consumption peak according to the decomposition of the β-PdH formed after reduction of bulk PdO²⁵ is not observed in our TPR experiments. This could be because large Pd particles readily lead to the formation of β-PdH,²⁶ while a good dispersion was achieved and small Pd particles were formed in these reported catalysts at a low loading of 0.8%. Pd/Al₂O₃ exhibits the lowest reduction temperature of Pd²⁺ species. The reduction profiles of PdM/Al₂O₃ catalysts migrate toward higher temperatures upon the increasing electropositivity of the additives, while the reduction temperature of PdXSr/Al₂O₃ samples shifts to higher temperatures more noticeably with an increase of Sr loading, implying that the doping of additives lowers the reducibility of Pd²⁺ species. The reduction temperature of Pd5Sr/Al₂O₃ is increased to 126 °C from 76 °C over the Pd/Al₂O₃ catalyst. From the reported data here, it is evident that a chemical interaction between the alkali earth metal ions and the supported Pd²⁺ precursor already exists at the low loading in PdM/Al₂O₃ catalysts, while this interaction becomes stronger with increasing Sr loading. Furthermore,

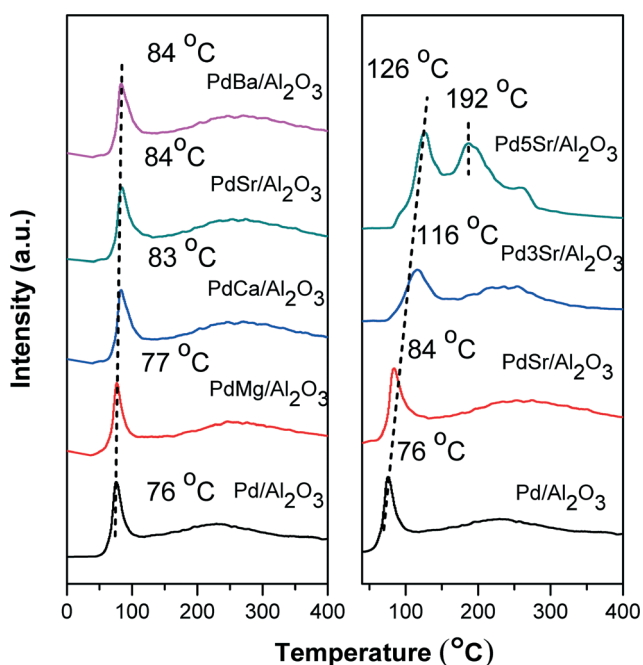


Fig. 2 TPR curves of the as-prepared PdM/Al₂O₃ and PdXSr/Al₂O₃ catalysts.

this chemical interaction also accounts for the promotion effect of the alkali earth metals for the Pd dispersion.

3.3.3 Acid–base properties: NH₃-TPD; CO₂-TPD. To measure the effect of alkali earth metals on surface acidity and basicity, NH₃-TPD (Fig. 3) and CO₂-TPD (Fig. 4) were performed.

The acid centers over the surface are believed to influence the catalytic performance of hydrogenolysis and etherification.²¹ NH₃-TPD measurements were carried out to examine the total acidity of the catalysts (Fig. 3). Normally, the area of a specific peak can be used to estimate the amount of ammonia desorbed from a sample, and it can be used as a standard to quantify the acidity of a sample.²⁷ A semi-quantitative comparison of the adsorption strength distribution was

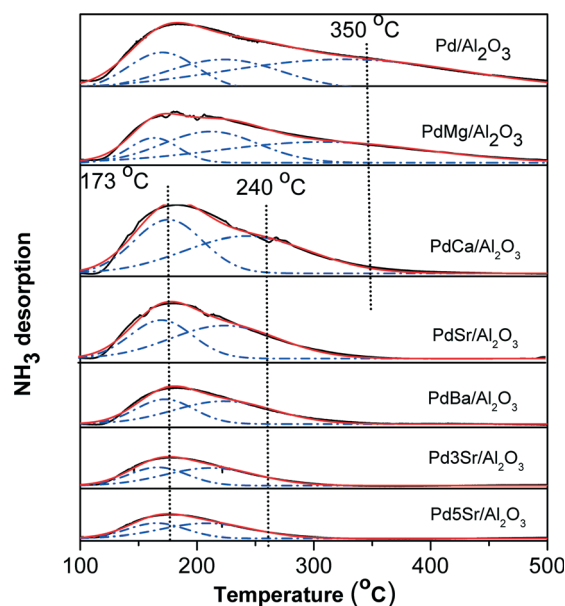


Fig. 3 NH₃-TPD profiles of the reduced catalysts.

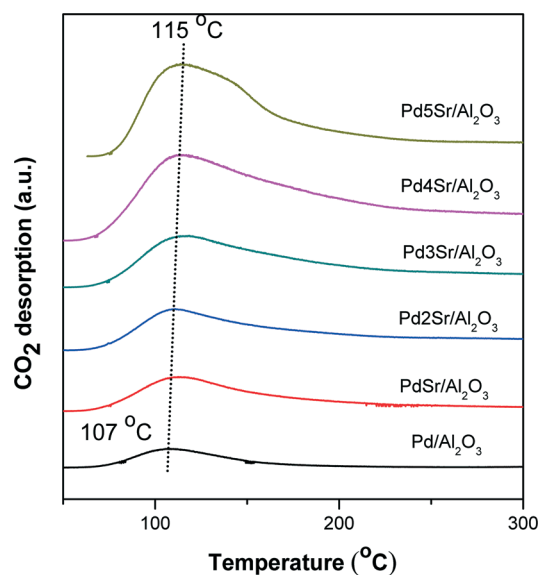


Fig. 4 CO₂-TPD profiles of the reduced catalysts.

achieved by deconvolution of peaks using a Gaussian function. The semi-quantitative results after multi-peak fitting are exhibited in Table 4. The addition of alkali earth metals to Pd/Al₂O₃ leads to a different extent of decrease in the amount of acid sites and acid strength. All samples showed a broad desorption peak with a maximum at 175–185 °C, which could be attributed to weak and medium acid sites. A shoulder on the high temperature side (320–350 °C) was observed over Pd/Al₂O₃ and PdMg/Al₂O₃ catalysts and was almost invisible over the PdCa/Al₂O₃ catalyst, which could be assigned to strong acid sites.²⁸ It can be observed in Fig. 3 that the addition of Mg reduces the intensity of strong acid sites, while the Ca-doping nearly neutralizes the strong acid sites completely judging from the high temperature desorption peak of NH₃. Furthermore, the high temperature desorption peak of NH₃ is attenuated further and disappears completely over PdBa/Al₂O₃ and PdXSr/Al₂O₃. The intensity of the broad peak is also reduced upon increasing the basic strength of the additives and is attenuated further with increasing Sr loading. In the deconvolution results displayed in Table 4, weak, medium and strong acids are designated as I, II, III respectively. All the peak temperatures over PdMg/Al₂O₃ are lower than those over Pd/Al₂O₃ indicating decreased acid strength. The peaks for strong acid sites took up too large a fraction in the deconvolution results, making direct comparison of the peak temperature of the weak and medium acid sites over PdMg/Al₂O₃ and PdCa/Al₂O₃ samples difficult. But the acid strength over PdCa/Al₂O₃ is weaker than that over PdMg/Al₂O₃ (Fig. 3), while the peaks of weak and medium acids shift to lower temperatures in the order: PdCa/Al₂O₃ > PdSr/Al₂O₃ = PdBa/Al₂O₃ > Pd3Sr/Al₂O₃ = Pd5Sr/Al₂O₃ (Table 4), indicating the decrease in acid strength. The total amount of acid sites reduces roughly in the same trend with the acid strength as estimated by the total area of NH₃ desorption peaks (Table 4). Upon increasing the Sr loading, the acid strength remarkably decreased initially (from PdSr/Al₂O₃ to Pd3Sr/Al₂O₃) and then remained nearly unchanged. The excess of Sr dopant could not weaken the acid strength further and only led to a slight decrease in the amount of acid sites. As the acidity of the catalysts is attributed to the Lewis acid sites of Al₂O₃ which accept electrons as evidenced by Pyridine-FTIR (see Fig. S6† for detail), the acidity changes of the samples could be ascribed to electron donation of the alkali earth metals to the Lewis acid sites in the Al₂O₃ support.

Table 4 Results of NH₃-TPD experiments over the catalysts

Catalyst	T _M (°C)			Total area (a.u.)	Peak fraction (%)		
	I	II	III		I	II	III
Pd/Al ₂ O ₃	170	223	350	23.0	19.4	25.9	54.8
PdMg/Al ₂ O ₃	163	212	320	17.8	14.4	35.2	50.5
PdCa/Al ₂ O ₃	173	240	—	16.1	40.9	59.2	—
PdSr/Al ₂ O ₃	171	223	—	14.3	37.7	62.3	—
PdBa/Al ₂ O ₃	173	222	—	8.4	37.6	62.4	—
Pd3Sr/Al ₂ O ₃	168	209	—	6.5	37.5	62.5	—
Pd5Sr/Al ₂ O ₃	168	207	—	4.8	39.7	60.3	—

In the CO₂-TPD profiles of the PdXSr/Al₂O₃ catalysts (Fig. 4), only one broad peak is obtained around 110–120 °C, corresponding to the weak basic sites. As the area of a specific peak could be used to evaluate the amount of base sites, it can be observed that the base amount increases upon an increase in Sr loading. Meanwhile, the peak due to CO₂ desorption shifts to a higher temperature (from 107 °C over Pd/Al₂O₃ to 115 °C over Pd5Sr/Al₂O₃), indicating a slight increase in base strength. As is expected, the acid strength and amount of acid sites decreased with increasing electropositivity of the doped-alkali earth metal and decreased further upon increasing Sr loading. On the contrary, the base strength and base amount increases with increasing Sr loading.

3.3.4 Adsorption characteristics: *in situ* CO-FTIR and furfural-FTIR. TPR experiments (*vide supra* section 3.3.2), which monitor the formation of Pd particles during the reduction process under H₂, manifest that the alkali earth metals have already interacted with the precursor Pd²⁺ phase. But still the question of whether the interaction still exists on the reduced Pd metal particle remains to be answered.²⁴ Furthermore, the adsorption properties of the poisoning CO on the metal surface is significantly important for the catalytic activity as CO is also produced during decarbonylation. In order to find out whether the doping phases still interact with the Pd particle and to understand in which way, CO was used as a probe molecule to examine the adsorption strength of CO and electronic states of Pd.

As showed in Fig. 5, the FTIR spectra exhibits four main peaks near 2086, 1989, 1936 and 1800–1900 cm⁻¹, which could be assigned to linear (band I), compressed-bridged (band II), isolated-bridged (band III)²⁹ and three-coordinated (band IV)³⁰ adsorption species of CO respectively. As band IV (1800–1900 cm⁻¹) is unusually broad, it can be attributed to different types of CO species on 3-fold hollow sites. The

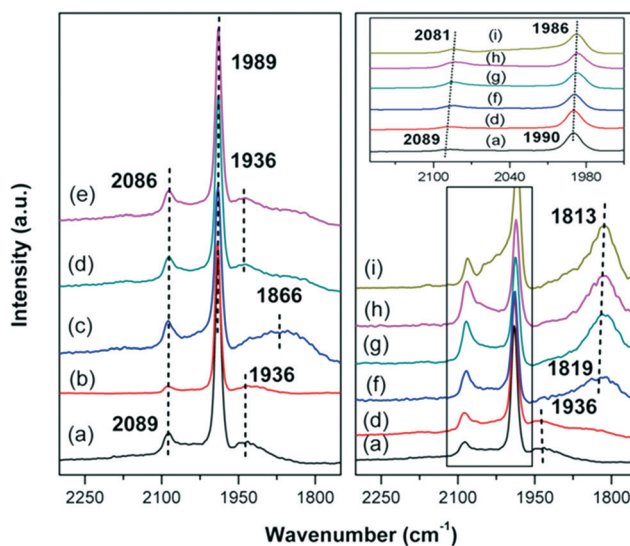


Fig. 5 *In situ* FTIR spectra of CO adsorbed on reduced catalysts: (a) Pd/Al₂O₃, (b) PdMg/Al₂O₃, (c) PdCa/Al₂O₃, (d) PdSr/Al₂O₃, (e) PdBa/Al₂O₃, (f) Pd2Sr/Al₂O₃, (g) Pd3Sr/Al₂O₃, (h) Pd4Sr/Al₂O₃, (i) Pd5Sr/Al₂O₃.

changes in CO spectra of PdM/Al₂O₃ with respect to Pd/Al₂O₃ can be rationalized in two main phenomena: (1) the additives result in a slight and gradual red shift of 3 cm⁻¹ upon the basic strength (Mg < Ca < Sr < Ba) for band I (from 2089 in Pd/Al₂O₃ to 2086 cm⁻¹ in PdBa/Al₂O₃). (2) A broad peak at 1866 cm⁻¹ indicating three-coordinated CO adsorption species appears over PdCa/Al₂O₃. This picture of the modification effect is enlarged by elevating the additive loading. The red shift upon increasing Sr loading is more obvious: (1) band II underwent a gradual downward shift of 4 cm⁻¹ (from 1990 cm⁻¹ in Pd/Al₂O₃ to 1986 cm⁻¹ in Pd5Sr/Al₂O₃), whereas band I underwent a progressive shift of 8 cm⁻¹ (from 2089 cm⁻¹ in Pd/Al₂O₃ to 2081 cm⁻¹ in Pd5Sr/Al₂O₃). (2) The isolated-bridged CO adsorption (1936 cm⁻¹) in Pd/Al₂O₃ transformed to stronger adsorption of CO on 3-fold hollow sites (1813–1819 cm⁻¹) upon increasing Sr loading and with a red shift of 6 cm⁻¹ from Pd2Sr/Al₂O₃ to Pd5Sr/Al₂O₃. It is evidently verified that the addition of low loading of alkali earth metals leads to a slight red shift of CO-FTIR and the elevated Sr loading results in increased red shift, which implies more remarkable strengthening of the Pd–CO bond.

Increased electron density on Pd was observed due to the addition of alkali ions to the Pd/SiO₂ catalyst,³¹ which caused increased red shift of all carbonyl bands, through a decreased bond order of C–O linkage resulting from the increased back-donation of electron density from Pd-3d orbits to the anti-bonding π molecular orbital of coordinated carbonyls. Inversely, the gradual red shift of CO-FTIR upon increase of Sr loading indicates the gradually increased electron intensity on metal Pd. A shift of 0.37 eV from Pd⁰ in Pd/Al₂O₃ (335.08 eV) to that in Pd3Sr/Al₂O₃ (334.71 eV) was observed by XPS (Fig. S7†). Electron donation from Sr or Ba species to the Pd⁽⁰⁾ (ref. 32) or Pd^(II) (ref. 33) was observed by XPS characterization. In summary, the electron intensity of metal Pd was gradually increased and the adsorption of CO was progressively strengthened upon increase of Sr loading while it was unnoticeable at low loadings of alkali earth metals.

The decarbonylation activity is also closely related to the adsorption properties of the carbonyl group. Moreover, the carbonyl group adsorption of HMF could also be influenced by the electron enrichment of metal Pd. But as HMF is difficult to vaporize with a high boiling point of 290 °C, furfural, which has a similar structure to HMF, was selected as a probe molecule to investigate the adsorption properties of the acyl group on PdXSr/Al₂O₃ catalysts. The profiles of furfural-FTIR are displayed in Fig. 6. To determine whether furfural could adsorb on the Al₂O₃ support and the added Sr species or not, and further to differentiate the C=O vibration of furfural adsorbed on different parts of the catalysts, we also carried out comparative tests over Al₂O₃ and 10% Sr loaded Al₂O₃ (designated as 5Sr/Al₂O₃) respectively. The assignment of the carbonyl-vibration peaks could be achieved as shown in Fig. 6a. The peak at 1718 cm⁻¹ is attributed to the carbonyl vibration of gaseous furfural, which could be regarded as being due to the physisorbed mode, similar to the dissolved cyclohexanone in the *in situ* ATR-IR.³⁴

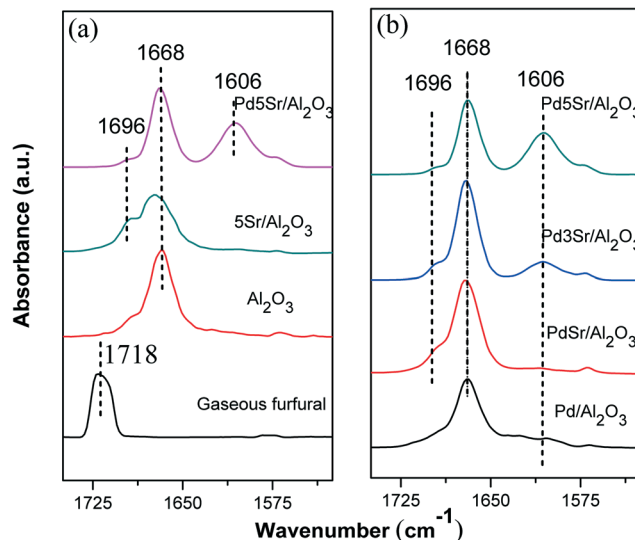


Fig. 6 *In situ* FTIR spectra of neat furfural and furfural adsorbed on reduced samples, adsorption for 10 min and evacuation for 5 min at 30 °C.

Therefore, no physisorbed mode of furfural on any of the samples exists as the carbonyl vibration shifts downward obviously on all the samples. The main peak at 1668 cm⁻¹ could be assigned to η^1 (O) adsorption on Al₂O₃ as is observed in the profile of Al₂O₃, which is similar to the reported adsorption of acetophenone on Al₂O₃.³⁴ By comparing with the profile of Al₂O₃, we favor the assignment of 1696 cm⁻¹ over 5Sr/Al₂O₃ to adsorption of carbonyl on Sr species. The electronegative carbonyl oxygen should bond to the electron-withdrawing Al₂O₃ more strongly than to the electron-enriched Sr species, leading to a higher vibration wavenumber over Sr species (1696 cm⁻¹) than over Al₂O₃ (1668 cm⁻¹). Compared with the profile of 5Sr/Al₂O₃, the newly appeared peak at 1605 cm⁻¹ over Pd5Sr/Al₂O₃ is attributed to the carbonyl adsorption on surface Pd, which may be tentatively assigned to the acyl adsorption through the η^1 (C) mode. A similar assignment was made for the peak at 1600 cm⁻¹ in the IR of acetophenone adsorption on Pd/Al₂O₃ when heated to 120 °C.³⁵ The acetyl species adsorbed on Pt (111) also exhibited a CO stretching frequency at 1600 cm⁻¹.³⁶ The η^2 configuration of the adsorbed acetophenone has been assigned at 1388 cm⁻¹ by the IR experiment with isotope-labeled acetophenone.³⁵ Fig. S8† shows the furfural-FTIR profile of Pd5Sr/Al₂O₃ evacuation at different temperature, with the η^2 adsorption of the carbonyl at 1365 cm⁻¹. A higher wavenumber indicates weaker adsorption of carbonyl group. With increase of evacuation temperature, the intensity of peaks at 1365 and 1605 cm⁻¹ increases, while peak at 1668 cm⁻¹ shows the adverse tendency, indicating gradual transformation of the carbonyl adsorption to stronger mode.

It is interesting to see that in Fig. 6b, the band at 1605 cm⁻¹ is nearly invisible over Pd/Al₂O₃ and PdSr/Al₂O₃ catalysts, while a clear signal is observed over Pd3Sr/Al₂O₃ and Pd5Sr/Al₂O₃ catalysts. What is more, the peak at 1605 cm⁻¹ intensifies with the increase of Sr loading, while the peak at 1668 cm⁻¹ shows the opposite trend. The band at 1696 cm⁻¹

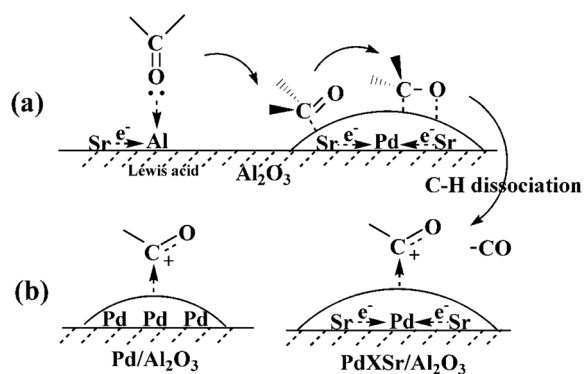
is very weak over all PdXSr/Al₂O₃ catalysts. We can conclude that a large amount of furfural is adsorbed on the Al₂O₃ support in η^1 (O) configuration initially, but gradually migrates to the Pd surface when heated, transforming to a stronger adsorption mode, namely η^1 (C) to η^2 (C, O). However, the added Sr species promoted the carbonyl adsorption on the Pd surface at low temperature probably through η^1 (C) configuration, which might be because of the increased electron density of Pd, thus the electronegative Pd is more liable to interact with the electropositive carbonyl carbon. Meanwhile, the increased electron enrichment on the Al₂O₃ support caused by Sr species (as discussed in 3.3.3) in turn weakens the carbonyl adsorption, as it is harder for the more electron rich Al₂O₃ to accept the lone pair donated from the carbonyl oxygen. Thus, a synergistic effect between the Sr species and metallic Pd is observed, that is, the electronic effect of the Sr species promotes the migration of furfural from the Al₂O₃ support to the Pd surface.

It was demonstrated that the decarbonylation process of aldehyde underwent C–H dissociation to form an acyl intermediate initially and then release CO.³⁷ As the metallic Pd with more electron enrichment could interact with the electropositive acyl carbon more strongly, the acyl intermediate of decarbonylation could be stabilized and thus its formation could be facilitated. In summary, the Sr species could promote the carbonyl migration from the support to the metallic Pd surface and facilitate the abstraction of the H atom to form the acyl intermediate (Scheme 2), which could lead to the promotion of decarbonylation activity.

4. Discussion

4.1 The effect of metallic surface area and the adsorption characteristics of metal Pd on the catalytic activity

Interaction between the alkali earth metals and Pd²⁺/Pd species before or after reduction is respectively evidenced by H₂-TPR (Fig. 2) and CO-FTIR (Fig. 5). As a result, Pd dispersion and metal surface area is promoted by addition of alkali earth metals as shown in Table 3. The electronic effect of the additives at low loading (over PdM/Al₂O₃ catalysts) is very



Scheme 2 Addition effect of Sr species on carbonyl adsorption and C–H dissociation.

weak as demonstrated by the CO-FTIR results. Therefore, the influence of the adsorption properties of CO and carbonyl group on the catalytic activity is negligible and the Pd dispersion or metal area would dominate over PdM/Al₂O₃ catalysts. The HMF conversion (in Table 2) and Pd dispersion (in Table 3) of PdM/Al₂O₃ show the same tendency: Pd/Al₂O₃ < PdMg/Al₂O₃ < PdCa/Al₂O₃ < PdSr/Al₂O₃ < PdBa/Al₂O₃. The promoted activity may be attributed to the increased metallic dispersion. This point is illustrated by the good linear correlation between the metallic Pd surface area and the catalysts' activity at low conversion (Fig. 7). The reaction rate at low conversion level could be roughly regarded as the initial activity. Among the different alkali earth metal-added catalysts, PdBa/Al₂O₃ with the highest metallic surface area ($S_{\text{Pd}} = 117.8 \text{ m}^2 \text{ g}^{-1}$) shows the highest HMF conversion. In contrast, Pd/Al₂O₃ shows the lowest HMF conversion due to its lowest metallic surface area ($S_{\text{Pd}} = 75.2 \text{ m}^2 \text{ g}^{-1}$). These results suggest that active sites for the decarbonylation reaction are located on reduced Pd and catalytic activity is closely associated with the amount of exposed metal area. Higher Pd dispersion or exposed metallic area would create more active sites, leading to higher initial activity over the catalyst.

It is noticed that Sr modification causes the decrease of specific area and pore size of Pd/Al₂O₃ catalyst (Table 3). Yet the decrease apparently did not reduce the initial activity of catalysts because all Sr added catalysts show better catalytic performance than Pd/Al₂O₃. Therefore, the initial activity of the catalysts appears to be solely linked to characteristics of Pd species, such as metal dispersion and electronic states. The HMF conversion of PdXSr/Al₂O₃ (in Table 2) initially increased with increasing Sr loading and then decreased after reaching a plateau. The relationship between the metallic Pd surface area and HMF conversion at low level is also shown

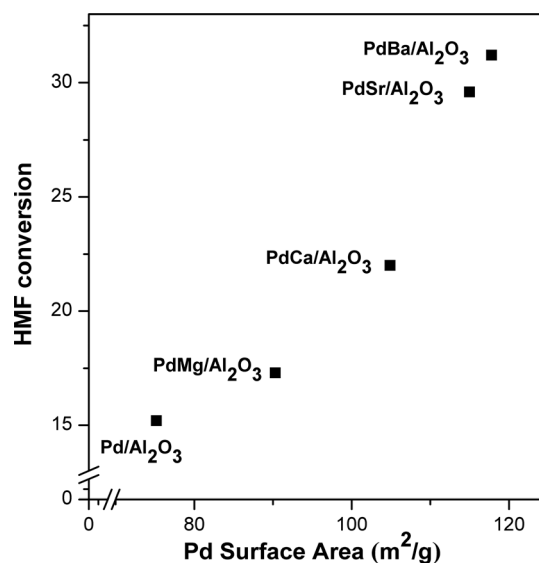


Fig. 7 Correlation between the metallic surface area and HMF conversion at low conversion. Conditions: 1.2 g HMF, 25 g 1,4-dioxane, 0.25 g catalyst, N₂ atmospheric pressure (room temperature), $T = 180 \text{ }^\circ\text{C}$, $t = 1 \text{ h}$.

in Fig. 8. The HMF conversion of PdXSr/Al₂O₃ at low level shows the same tendency with that at high conversion level in Table 2. The HMF conversion initially increases until reaching a plateau at a moderate Sr content and then decreases with further elevation of Sr loading, while the metallic surface area increases all the time with an increase in Sr loading. It can be concluded that besides the increase of metal area, the initial activity of PdXSr/Al₂O₃ catalysts is meanwhile influenced by other characteristics of metal Pd. As discussed in 3.3.4, the Sr additive could promote the carbonyl adsorption and C–H dissociation on the metallic Pd surface to form the acyl intermediate, the decarbonylation activity could be increased with increase of Sr loading initially. However, CO is produced during decarbonylation and the adsorption of the poisoning CO on the catalysts strengthens with the increasing Sr content as evidenced by the CO-FTIR, which would result in the occupancy of the active metal sites. When the strengthening adsorption of CO dominates among the conflicting factors, decarbonylation activity would decrease. Therefore, a peak value of HMF conversion appeared at a moderate loading of Sr species as exhibited in Table 2 and Fig. 8.

4.2 Relationships between the product selectivity and the catalyst acidity

Hydrogenolysis usually goes through two steps: dehydration and hydrogenation.³⁸ In some studies, acidic solids for instance H₂WO₄,³⁹ and ion-exchange resins^{38,40} were added to the reaction system to promote the initial dehydration of glycerol. I. Gandarias *et al.*⁴¹ have studied the role of acid and metal sites of Pt/ASA in glycerol hydrogenolysis and found that ASA acid sites catalyzed the dehydration of glycerol to acetol while Pt metal sites were responsible for acetol

hydrogenation. Our group have found that the concentration of Brønsted acid sites appeared to be a key to the glycerol selective hydrogenolysis to 1,3-propanediol, whereas the concentration of Lewis acid sites were related to the formation of 1,2-propanediol.⁴² In this respect, the acidic support Al₂O₃ can promote dehydration and consequently hydrogenolysis over the Pd/Al₂O₃ catalyst. Meanwhile, Lewis acids can also catalyze the etherification reaction of primary, secondary, and tertiary alcohols effectively through direct dehydration of alcohols.^{21c,43} For example, diethyl ether can be synthesized in high yield through vapor-phase dehydration of ethanol on an alumina catalyst.⁴⁴

According to the pyridine-FTIR and the NH₃-TPD results, there is an effect of electron donation from alkali earth metal species to the Lewis acid sites of the Al₂O₃ support. As a result, both the acid strength and amount of acid sites on the support is attenuated at different extents dependent on the basic strength of the additives and the additive (Sr) loading. As shown in Fig. 9, along with the decrease of total acid amount brought about by the addition of alkali earth metal, the hydrogenolysis and etherification selectivity decreases though with a decreasing slope over PdXSr/Al₂O₃ catalysts. The decrease of the slope is derived from the decreased acid strength, as which strong acid could promote hydrogenolysis and etherification largely and the decrease of medium and weak acid sites suppresses the side reactions in a slower speed. Contrary to the side products, FOL selectivity is increased progressively with a decrease of acidity. However, though the amount of acid sites decreased further over Pd4Sr/Al₂O₃ to Pd5Sr/Al₂O₃, the hydrogenolysis and etherification side reactions are suppressed slightly, as the very small amount of the side products may be solely linked to the metallic Pd. The selectivity of FAL shows the same tendency as that of hydrogenolysis products (Table 2), which

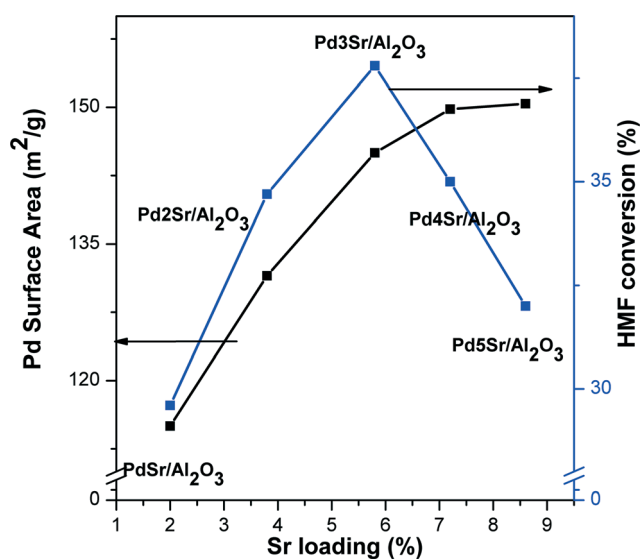


Fig. 8 Pd surface area and HMF conversion as a function of Sr loading at low conversion. Conditions: 1.2 g HMF, 25 g 1,4-dioxane, 0.25 g catalyst, N₂ atmospheric pressure (room temperature), T = 180 °C, t = 1 h.

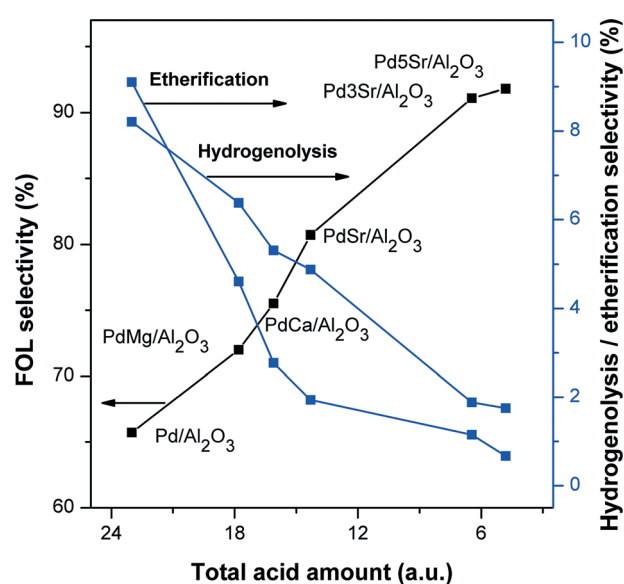


Fig. 9 The selectivity of FOL, hydrogenolysis and etherification products as a function of total amount of acid sites.

may also be brought about by the acidity changes of the catalysts. In all, the addition of alkali earth metal species weakens the acid strength and amount of acid sites of Pd/Al₂O₃ and subsequently suppresses hydrogenolysis and etherification side reactions.

5. Conclusion

Depending on the alkali earth metal category and additive loading, the modified Pd/Al₂O₃ demonstrates remarkably enhanced catalytic performance. In the Pd/Al₂O₃ catalytic system, a newly extensive product distribution is formed with hydrogenolysis and etherification as the main side reactions. As is expected, the doping of alkali earth metals attenuates the acid strength as well as the amount of acid sites of the catalysts, resulting in the suppression of hydrogenolysis and etherification side reactions. On the other hand, the low loading of Mg, Ca, Sr, Ba improves surface Pd dispersion, leading to an initial promotion of activity over PdM/Al₂O₃ catalysts. The promotion effect increases with increased Sr content. However, the decarbonylation activity is not only determined by the metal sites when Sr content increases over PdXSr/Al₂O₃ catalysts, but also greatly influenced by the adsorption properties of the carbonyl and the poisoning CO released. We demonstrate that with an increase in Sr loading, an acyl species adsorbed on surface Pd appears, which indicates the migration of carbonyl adsorption from the support to the surface Pd. A synergistic effect between the Sr species and the metal Pd on the carbonyl adsorption is clarified through the electron donation of Sr species to Al₂O₃ and metallic Pd. Moreover, the increased electron density of Pd could also promote the C–H dissociation of aldehyde to form the acyl intermediate. Thus, the decarbonylation activity could increase with increased Sr content. But the adsorption of the produced CO also strengthens with an increase in Sr loading, therefore delaying the release of active metal sites, hindering decarbonylation. As a result, HMF conversion increases with an increase in Sr loading until it reaches a peak value at a moderate Sr loading and then decreases with further elevation of Sr loading. The initial activity and decarbonylation selectivity over Pd3Sr/Al₂O₃ is increased by 30% and 25% respectively, compared with that over Pd/Al₂O₃. Moreover, an optimized FOL yield of 92% is achieved by gas exchange in the period of reaction over Pd3Sr/Al₂O₃.

Acknowledgements

The authors gratefully acknowledge the financial support of the Major State Basic Research Development Program of China (973 Program) (no. 2012CB215305). We would like to thank Dr. Hongyan Zheng for helpful discussions.

References

- (a) G. W. Huber and J. A. Dumesic, *Catal. Today*, 2006, **111**, 119–132; (b) J. N. Chheda, G. W. Huber and J. A. Dumesic, *Angew. Chem., Int. Ed.*, 2007, **46**, 7164–7183; (c) D. M. Alonso, J. Q. Bond and J. A. Dumesic, *Green Chem.*, 2010, **12**, 1493; (d) T. D. Matson, K. Barta, A. V. Iretskii and P. C. Ford, *J. Am. Chem. Soc.*, 2011, **133**, 14090–14097.
- (a) J. N. Chheda and J. A. Dumesic, *Catal. Today*, 2007, **123**, 59–70; (b) J. N. Chheda, G. Huber and J. A. Dumesic, *Angew. Chem., Int. Ed.*, 2007, **46**, 7164–7183; (c) J. S. Luterbacher, D. Martin Alonso and J. A. Dumesic, *Green Chem.*, 2014, **16**, 4816–4838; (d) A. Corma, S. Iborra and A. Velty, *Chem. Rev.*, 2007, **107**, 2411–2502; (e) B. Peng, X. Yuan, C. Zhao and J. A. Lercher, *J. Am. Chem. Soc.*, 2012, **134**, 9400–9405; (f) A. Fukuoka and P. L. Dhepe, *Angew. Chem., Int. Ed.*, 2006, **45**, 5161–5163.
- (a) G. W. Huber, S. Iborra and A. Corma, *Chem. Rev.*, 2006, **106**, 4044–4098; (b) S. Wesselbaum, T. Vom Stein, J. Klankermayer and W. Leitner, *Angew. Chem., Int. Ed.*, 2012, **51**, 7499–7502; (c) R. Rinaldi and F. Schüth, *Energy Environ. Sci.*, 2009, **2**, 610.
- (a) G. W. Huber, J. N. Chheda, C. J. Barrett and J. A. Dumesic, *Science*, 2005, **308**, 1446–1450; (b) C. Barrett, J. Chheda, G. Huber and J. Dumesic, *Appl. Catal., B*, 2006, **66**, 111–118; (c) M. Chidambaram and A. T. Bell, *Green Chem.*, 2010, **12**, 1253; (d) T. Thananathanachon and T. B. Rauchfuss, *Angew. Chem., Int. Ed.*, 2010, **49**, 6616–6618; (e) R. Alamillo, M. Tucker, M. Chia, Y. Pagán-Torres and J. Dumesic, *Green Chem.*, 2012, **14**, 1413; (f) Y. Nakagawa, M. Tamura and K. Tomishige, *ACS Catal.*, 2013, **3**, 2655–2668.
- (a) H. Li, S. Zhang and H. Luo, *Mater. Lett.*, 2004, **58**, 2741–2746; (b) B. Nagaraja, A. Padmasri, B. D. Raju and K. R. Rao, *J. Mol. Catal. A: Chem.*, 2007, **265**, 90–97; (c) R. S. Rao, R. T. K. Baker and M. A. Vannice, *Catal. Lett.*, 1999, **60**, 51–57; (d) M. Villaverde, N. Bertero, T. Garetto and A. Marchi, *Catal. Today*, 2013, **213**, 87–92; (e) R. V. Sharma, U. Das, R. Sammynaiken and A. K. Dalai, *Appl. Catal., A*, 2013, **454**, 127–136.
- (a) A. Corma, O. de la Torre, M. Renz and N. Vollandier, *Angew. Chem., Int. Ed.*, 2011, **50**, 2375–2378; (b) A. Corma, O. de la Torre and M. Renz, *ChemSusChem*, 2011, **4**, 1574–1577.
- Y. Su, H. M. Brown, X. Huang, X.-D. Zhou, J. E. Amonette and Z. C. Zhang, *Appl. Catal., A*, 2009, **361**, 117–122.
- (a) G. Lv, H. Wang, Y. Yang, X. Li, T. Deng, C. Chen, Y. Zhu and X. Hou, *Catal. Sci. Technol.*, 2016, DOI: 10.1039/C5CY01149C; (b) Z. Miao, Y. Zhang, X. Pan, T. Wu, B. Zhang, J. Li, T. Yi, Z. Zhang and X. Yang, *Catal. Sci. Technol.*, 2015, **5**, 1314–1322; (c) N. Mei, B. Liu, J. Zheng, K. Lv, D. Tang and Z. Zhang, *Catal. Sci. Technol.*, 2015, **5**, 3194–3202.
- A. S. Nagpure, A. K. Venugopal, N. Lucas, M. Manikandan, R. Thirumalaiswamy and S. Cilukuri, *Catal. Sci. Technol.*, 2015, **5**, 1463–1472.
- F. Yang, S. Zhang, Z. C. Zhang, J. Mao, S. Li, J. Yin and J. Zhou, *Catal. Sci. Technol.*, 2015, **5**, 4602–4612.
- L. D. Lillwitz, US4089871A, 1978.
- F. M. A. Geilen, T. V. Stein, B. Engendahl, S. Winterle, M. A. Liauw, J. Klankermayer and W. Leitner, *Angew. Chem., Int. Ed.*, 2011, **50**, 6831–6834.
- Y.-B. Huang, Z. Yang, M.-Y. Chen, J.-J. Dai, Q.-X. Guo and Y. Fu, *ChemSusChem*, 2013, **6**, 1348–1351.

- 14 J. Mitra, X. Zhou and T. Rauchfuss, *Green Chem.*, 2015, **17**, 307–313.
- 15 (a) W. Zhang, Y. Zhu, S. Niu and Y. Li, *J. Mol. Catal. A: Chem.*, 2011, **335**, 71–81; (b) H. Zhang, X.-K. Gu, C. Canlas, A. J. Kropf, P. Aich, J. P. Greeley, J. W. Elam, R. J. Meyers, J. A. Dumesic, P. C. Stair and C. L. Marshall, *Angew. Chem., Int. Ed.*, 2014, **53**, 12132–12136.
- 16 L. Bai, Y. Zhou, Y. Zhang, H. Liu and M. Tang, *Catal. Lett.*, 2009, **129**, 449–456.
- 17 B. Zhang, Y. Zhu, G. Ding, H. Zheng and Y. Li, *Appl. Catal., A*, 2012, **443–444**, 191–201.
- 18 (a) A. Gluhoi, N. Bogdanchikova and B. Nieuwenhuys, *J. Catal.*, 2005, **232**, 96–101; (b) A. C. Gluhoi and B. E. Nieuwenhuys, *Catal. Today*, 2007, **122**, 226–232.
- 19 M. G. Musolino, C. V. Caia, C. Busacca, F. Mauriello and R. Pietropaolo, *Appl. Catal., A*, 2009, **357**, 106–113.
- 20 V. V. Pushkarev, N. Musselwhite, K. An, S. Alayoglu and G. A. Somorjai, *Nano Lett.*, 2012, **12**, 5196–5201.
- 21 (a) Y. Nakagawa, X. Ning, Y. Amada and K. Tomishige, *Appl. Catal., A*, 2012, **433**, 128–134; (b) Y. Kusunoki, T. Miyazawa, K. Kunimori and K. Tomishige, *Catal. Commun.*, 2005, **6**, 645–649; (c) A. Corma and M. Renz, *Angew. Chem.*, 2007, **119**, 302–304.
- 22 (a) S. Damyanova, B. Pawelec, K. Arishtirova, J. L. G. Fierro, C. Sener and T. Dogu, *Appl. Catal., B*, 2009, **92**, 250–261; (b) M. Souza, D. A. G. Aranda and M. Schmal, *J. Catal.*, 2001, **204**, 498–511.
- 23 (a) C. Shi and P. Zhang, *Appl. Catal., B*, 2015, **170**, 43–52; (b) L. M. Gomez-Sainero, X. L. Seoane, J. L. G. Fierro and A. Arcoya, *J. Catal.*, 2002, **209**, 279–288; (c) J. Wan, R. Ran, X. Wu, Y. Cao, M. Li, D. Weng and K. Huang, *Catal. Today*, 2015, **253**, 51–56.
- 24 R. Pellegrini, G. Leofanti, G. Agostini, L. Bertinetti, S. Bertarione, E. Groppo, A. Zecchina and C. Lamberti, *J. Catal.*, 2009, **267**, 40–49.
- 25 (a) S. C. Shekar, J. K. Murthy, P. K. Rao and K. S. R. Rao, *J. Mol. Catal. A: Chem.*, 2003, **191**, 45–59; (b) S. Bhogeswararao and D. Srinivas, *J. Catal.*, 2015, **327**, 65–77.
- 26 H. Chen, Z. Xu, H. Wan, J. Zheng, D. Yin and S. Zheng, *Appl. Catal., B*, 2010, **96**, 307–313.
- 27 D. Ma, W. Zhang, Y. Shu, X. Liu, Y. Xu and X. Bao, *Catal. Lett.*, 2000, **66**, 155–160.
- 28 C. Yu, Q. Ge, H. Xu and W. Li, *Appl. Catal., A*, 2006, **315**, 58–67.
- 29 W. Kim, *Appl. Catal., A*, 2004, **268**, 77–82.
- 30 S. Bertarione, D. Scarano, A. Zecchina, V. Johanek, J. Hoffmann, S. Schaueremann, M. M. Frank, J. Libuda, G. Rupprechter and H. J. Freund, *J. Phys. Chem. B*, 2004, **108**, 3603–3613.
- 31 V. Pitchon, M. Guenin and H. Praliaud, *Appl. Catal.*, 1990, **63**, 333–343.
- 32 E. Ding, S. Jujjuri, M. Sturgeon, S. G. Shore and M. A. Keane, *J. Mol. Catal. A: Chem.*, 2008, **294**, 51–60.
- 33 T. Kobayashi, T. Yamada and K. Kayano, *Appl. Catal., B*, 2001, **30**, 287–292.
- 34 C. Kereszszegi, D. Ferri, T. Mallat and A. Baiker, *J. Catal.*, 2005, **234**, 64–75.
- 35 H. W. Chen, C. S. Chen and S. J. Harn, *J. Phys. Chem.*, 1995, **99**, 10557–10564.
- 36 G. Mitchell, P. Radloff, C. Greenlief, M. Henderson and J. White, *Surf. Sci.*, 1987, **183**, 403–426.
- 37 (a) J. Davis and M. Barteau, *J. Am. Chem. Soc.*, 1989, **111**, 1782–1792; (b) M. Mavrikakis and M. A. Barteau, *J. Mol. Catal. A: Chem.*, 1998, **131**, 135–147; (c) R. Shekhar, M. A. Barteau, R. V. Plank and J. M. Vohs, *J. Phys. Chem. B*, 1997, **101**, 7939–7951; (d) S. Sitthisa, T. Pham, T. Prasomsri, T. Sooknoi, R. G. Mallinson and D. E. Resasco, *J. Catal.*, 2011, **280**, 17–27.
- 38 T. Miyazawa, Y. Kusunoki, K. Kunimori and K. Tomishige, *J. Catal.*, 2006, **240**, 213–221.
- 39 J. Chaminand, L. aurent Djakovitch, P. Gallezot, P. Marion, C. Pinel and C. Rosier, *Green Chem.*, 2004, **6**, 359–361.
- 40 T. Miyazawa, S. Koso, K. Kunimori and K. Tomishige, *Appl. Catal., A*, 2007, **329**, 30–35.
- 41 I. Gandarias, P. L. Arias, J. Requies, M. B. Güemez and J. L. G. Fierro, *Appl. Catal., B*, 2010, **97**, 248–256.
- 42 S. Zhu, Y. Qiu, Y. Zhu, S. Hao, H. Zheng and Y. Li, *Catal. Today*, 2013, **212**, 120–126.
- 43 (a) H. Firouzabadi, N. Iranpoor and A. A. Jafari, *J. Mol. Catal. A: Chem.*, 2005, **227**, 97–100; (b) S. Kim, K. N. Chung and S. Yang, *J. Org. Chem.*, 1987, **52**, 3917–3919.
- 44 (a) R. Clark, W. Graham and A. Winter, *J. Am. Chem. Soc.*, 1925, **47**, 2748–2754; (b) F. F. Roca, L. De Mourgues and Y. Trambouze, *J. Catal.*, 1969, **14**, 107–113.